Coupled diffusion–fabric-flow phenomena: an effective stress analysis

M. Fam and J.C. Santamarina

Abstract: Concentration diffusion, fluid flow and fabric changes are coupled phenomena in fine soils. Indeed, experimental results previously presented by the authors showed the presence of a pressure front advancing ahead of the diffusing high-concentration front in bentonite and kaolinite specimens. This note presents a simple analysis of diffusion–fabric-flow coupling, based on elementary double-layer repulsion and attraction. Model predictions adequately agree with experimental data. High specific surface, high initial void ratio, and low initial pore-fluid concentration increase the sensitivity of soils to changes in pore-fluid concentration and enhance the potential development of pore pressure fronts.

Key words: coupling, diffusion, clay, pore pressure, interparticle forces.

Résumé : La diffusion de concentration, l'écoulement du fluide et les changements de fabrique sont des phénomènes couplés dans les sols fins. En effet, des résultats expérimentaux présentés antérieurement par les auteurs indiquent la présence d'un front de pression qui progresse en avant du front de forte concentration diffusant dans des spécimens de bentonite et kaolin. Cette note présente une simple analyse du couplage diffusion–fabrique-écoulement basée sur la répulsion et l'attraction élémentaires de la double-couche. Les prédictions du modèle concordent adéquatement avec les données expérimentales. Une surface spécifique élevée, un rapport de vide initial élevé et une forte concentration initiale du fluide interstitiel accroît la sensibilité des sols aux changements de concentration du fluide interstitiel et favorise le développement de fronts de pression interstitielle.

Mots clés : couplage, diffusion, argile, pression interstitielle, forces interparticules.

[Traduit par la rédaction]

Introduction

A change in chemical boundary conditions produces a diffusion front that gradually changes the pore fluid surrounding soil particles. These changes affect interparticle forces, and may lead to volumetric strains and changes in strength. The coupling of these phenomena are not uncommon; it occurs in natural systems (e.g., marine clays becoming quick clays) and in man-made systems (e.g., dam cores during the filling of reservoirs and clay liners subjected to contaminants).

Experiments conducted by the authors on kaolinite and bentonite, within a modified oedometric cell, have shown that concentration fronts produce volumetric changes and pore pressure fronts (Santamarina and Fam 1995). The purposes of this note are to capture intervening phenomena in a simple mathematical framework, to understand the relative role of participating soil parameters, and to assess the predictive capabilities of the model. This study starts with a review of effective stress definitions in saturated soils.

Received December 6, 1995. Accepted January 7, 1996.

M. Fam. Civil Engineering Department, University of Waterloo, Waterloo, ON N2L 3G1, Canada.

J.C. Santamarina.[1] School of Civil and Environmental Engineering, Georgia Institute of Technology, Atlanta, GA 30332-0355, U.S.A.

[1] Former address: University of Waterloo, Waterloo, Ont., Canada.

Effective stress models

The failure of continuum mechanics to explain soil phenomena motivated the analysis of soil systems at increasingly smaller scales. The concept of effective stress was introduced to compute shear strength and volume change in particulate materials. Mathematically, Terzaghi's effective stress σ' is expressed as (Terzaghi 1936)

$$[1] \quad \sigma' = \sigma - u$$

where σ is the total applied stress and u is the pore-fluid pressure. Terzaghi's generalized description of the stress acting on the soil skeleton has allowed for the unified interpretation of drained and undrained behavior under normal loading conditions.

Several limitations to Terzaghi's effective stress have been recognized. Consequently, alternative definitions have been proposed for coarse-grained particulate materials and for fine-grained particulate systems that are sensitive to electrical–chemical factors. These definitions are summarized in Table 1. A brief discussion follows.

Coarse soils

Terzaghi's principle reflects force balance. From a deformation point of view, particles and fluid are incompressible, and measured strains are due to changes in pore geometry

Table 1. Classical effective stress models (saturated media).

Reference	Expression	Notes
Coarse soil		
Terzaghi (1936)	$\sigma' = \sigma - u$	Empirical shear strength
Skempton (1960)	$\sigma' = \sigma - u\left(1 - a\frac{\tan\psi}{\tan\phi}\right)$	Shear strength
Biot (1941); Skempton (1960); Nur and Byerlee (1971)	$\sigma' = \sigma - u\left(1 - \frac{C_s}{C}\right)$	Compressibility
Fine soil		
Lambe (1960)	$\sigma' \equiv \sigma - u = \sigma_c + (R_{DL} - \text{Att})$	Shear strength (constant volume)
Bolt (1956)	$\sigma' \equiv \sigma - u = (R_{DL} - \text{Att})$	Series model; no material contact (equal stress in solid and double layer)
Sridharan and Rao (1973)	$\sigma' \equiv \sigma_c = \sigma - u - (R_{DL} - \text{Att})$	Strain compatibility; parallel model (equal deformation in solid and double layer)

Notes: $\equiv$ indicates definition; σ, total stress; σ', effective stress; σ_c, intergranular pressure or short-range stress at contact; u, water pressure; R_{DL}, double-layer repulsion; Att, interparticle attraction; a, area of contact between particles per unit area of material; C_s, bulk compressibility of the material of particles; C, bulk compressibility of the dry soil; ϕ, friction angle; ψ, angle of intrinsic friction between particles.

and grain rupture (Carroll and Katsube 1983). Skempton's model of effective stress for volume change considers compressible particles but incompressible pore fluid (Table 1; Skempton 1960; Oka 1988). Biot's poroelastic theory accounts for the compressibility of both fluid and solid components. It is worth noting that the change in pore pressure in a poroelastic mass under three-dimensional loading may exceed the total stress increment (Cryer 1963; Chopra and Dargush 1995). The difference in pore pressure between Terzaghi's and Biot's theories depends on the elastic constants of the poroelastic medium.

Skempton's definition of effective stress for shear strength depends on the intrinsic angle of interparticle friction ψ. However, experimental results by Skinner (1969; see also Ishibashi et al. 1994) indicate that there is no effect of the intrinsic angle of interparticle friction ψ on the angle of shear resistance of the soil ϕ. While particle rolling may explain this observation, the evidence is not conclusive.

Fine soils

Electrical forces

Changes in pore-fluid valence, concentration, permittivity, or temperature have insignificant effects on the properties of coarse soils (low-strain damping due to squirting is a possible exception; see Spencer 1981). However, changes in fluid characteristics have crucial implications in the behavior of fine-grained geomaterials, altering shear strength and producing volumetric strains.

The study of electrical forces is conducted at different scales. Long-range repulsion and attraction are considered when the distance between particles exceeds ~20 Å (1Å = 0.1 nm) (Hueckel 1992). At closer distance, molecular and interatomic forces are analyzed (e.g., Born repulsion, hydration, and chemical bonding). In some soils, material contacts (or short-range forces) and long-range forces may coexist at a contact (e.g., kaolinite). There are also soils where the only participating forces are long range (e.g., bentonite at low confinement).

The long-range double-layer repulsion stress between parallel particles R_{DL} can be estimated from the osmotic pressure between the pore-fluid concentration and the ionic concentration between particles. Two solutions can be found depending on the interparticle distance (Santamarina and Fam 1995):

$$[2] \quad R_{DL} = 2RTc\left(2\pi^2\frac{\vartheta^2}{d^2} - 1\right)$$

short interparticle distance

$$[3] \quad R_{DL} = 64(RTc)e^{-(d/\vartheta)}$$

large interparticle distance

The interparticle spacing d is related to the void ratio e through specific surface A_s, specific gravity G_s, and mass density of water ρ_w:

$$[4] \quad d = \frac{2e}{A_s G_s \rho_w}$$

The "double layer thickness" ϑ is obtained from Gouy-Chapman theory (Mitchell 1993):

$$[5] \quad \vartheta = \sqrt{\frac{\varepsilon_o \kappa' RT}{2F^2 c v^2}}$$

Other parameters involved in these relationships are as follows: pore-fluid concentration c, valence of the prevailing ion v, relative dielectric permittivity of the pore fluid κ', temperature T, permittivity of vacuum $\varepsilon_o = 8.86 \times 10^{-12}$ F/m, gas constant $R = 8.314$ J·mol^{-1}·K^{-1}, and Faraday's constant $F = 9.65 \times 10^4$ C/mol.

The dimensionless ratio $X = d/\vartheta$ between interparticle spacing and double-layer thickness is used to differentiate between short and large interparticle spacing: $d/\vartheta < 2$ indicates short interparticle spacing, whereas $d/\vartheta > 3$ implies large interparticle distance. These limits are compatible with assumptions imposed during the derivation of eq. 2 and eq. 3.

The long-range interparticle attraction can be approximated by London's theory as (Israelachvili 1991)

$$[6] \quad \text{Att} = \frac{A}{6\pi d^3}$$

The Hamaker constant A is slightly sensitive to changes in concentration (Santamarina and Fam 1995). Typical values of A for mineral–electrolyte systems vary between 10^{-20} and 10^{-21} J.

Once electrical forces are known, the definition of effective stress (eq. 1) can be modified to take into consideration the coparticipation of electrical forces with material–contact forces. Either a series model (equal forces) or a parallel model (equal deformation) can be assumed. The change in effective stress $\Delta\sigma'$ in the *series model* is equal to the change in the electrochemical stress ($\Delta R_{DL} - \Delta\text{Att}$) (Bolt 1956; Hueckel 1992),

$$[7] \quad \Delta\sigma' = \Delta\sigma - \Delta u = \Delta R_{DL} - \Delta\text{Att} \quad \text{(series model)}$$

and the total strain is the sum of the strain in particles and the strain in double layers. This model can adequately describe volumetric strains for parallel particle packings or very fine dispersed soils such as bentonite. The increase in shear strength with normal stress in the series model could be attributed to the decrease in water mobility towards the particle surface; yet, Allam and Sridharan (1984) argued that viscosity alone cannot explain the measured shear strength. Random particle orientation, short-range interparticle forces, and the formation of the Stern layer are not considered in this model. Further discussion of limitations can be found in Israelachvili (1991).

Compatibility of deformations in *parallel models* enforces the deformation in double layers to be equal to the deformation in contacts (Sridharan and Rao 1973). The change in effective stress becomes

$$[8] \quad \Delta\sigma' = \Delta\sigma - \Delta u - (\Delta R_{DL} - \Delta\text{Att}) \text{(parallel model)}$$

Changes in shear strength due to changes in pore fluid at constant confining stress are readily explained with this model. Alternatively, the parallel model by Lambe (1960; Table 1) can be adopted to explain changes in shear strength with changes in pore-fluid chemistry at constant strain (Yong and Warkentin 1966).

Barbour and Fredlund (1989) proposed the use of the osmotic pressure as a more robust state variable, and defined their model at the macroscale. The elementary approach selected in this study, on the basis of $R_{DL} - \text{Att}$, permits relating the analytical solution to micro-level parameters, allowing better insight into the relative role of participating variables. However, upscaling micro models, from the particle level to the macro soil mass is not immediate. The formation of granularities and fabric features at different scales add significant complexity. For example, the observed macro-level behavior of most clays appears as a mixture of both series and parallel models.

Coupled diffusion–fabric-flow

The derivation of the partial differential equation for diffusion–fabric-flow coupling begins assuming continuity and Darcy's law, as in Terzaghi's one-dimensional consolidation theory:

$$[9] \quad \frac{\partial\sigma'}{\partial t} = -\frac{k}{m_v\gamma_w}\frac{\partial^2 u_z}{\partial z^2} = -c_v\frac{\partial^2 u_z}{\partial z^2}$$

(effective stress ↔ flow)

where k is the coefficient of permeability, m_v is the coefficient of volume compressibility, t is time, γ_w is the unit weight of the fluid, z is the direction of the flow, and c_v is the coefficient of consolidation. The effective stress definition proposed in eq. 8 (parallel model) is selected on the basis of previous results for bentonite, which suggest that the effective stress increases during concentration diffusion (Santamarina and Fam 1995). Assuming constant confining stress σ, the change in effective stress with time is (from eq. 8)

$$[10] \quad \frac{\partial\sigma'}{\partial t} = -\frac{\partial u}{\partial t} - \frac{\partial R_{DL}}{\partial t} + \frac{\partial\text{Att}}{\partial t} \quad \text{(fluid ↔ effective stress)}$$

substituting eq. 10 in eq. 9,

$$[11] \quad \frac{\partial u}{\partial t} + \frac{\partial R_{DL}}{\partial t} - \frac{\partial\text{Att}}{\partial t} = c_v\frac{\partial^2 u_z}{\partial z^2}$$

The change in repulsion and attraction forces is computed from eq. 2 or 3 and 6 (see Appendix A), and the following differential equation is obtained:

$$[12] \quad \frac{\partial u}{\partial t} = c_v(1+\beta-\gamma)\frac{\partial^2 u}{\partial z^2} + \delta RT\frac{\partial c}{\partial t}$$

(fluid ↔ fabric ↔ flow)

Coefficients β and δ depend on the ratio $X = d/\vartheta$ and the characteristics of the mineral–fluid system. For short interparticle spacing, ($d/\vartheta < 2$)

$$[13] \quad \beta = 16\pi^2\alpha X^{-3} \quad \text{where} \quad \alpha = ca_v RT(A_s G_s \rho_w \vartheta)^{-1}$$

and

$$[14] \quad \delta = 2$$

For large interparticle spacing ($d/\vartheta > 3$)

$$[15] \quad \beta = 128\alpha e^{-X}$$

and

$$[16] \quad \delta = 64\left(\frac{X}{2} - 1\right)e^{-x}$$

The parameter γ captures the effect of the change in van der Waals attraction

$$[17] \quad \gamma = \frac{a_v A}{\pi A_s G_s \rho_w (X\vartheta)^4}$$

Typical values of the dimensionless coefficients β, γ, and δ were computed for the bentonite clay used in this study (Table 2) and are plotted in Fig. 1 for short and large interparticle spacings. The coefficient γ is small relative to β ($\gamma \approx 0.01\beta$), and it can be neglected in the analysis; this implies that the change in repulsion forces prevails over the change in attraction forces in this mineral–fluid system.

Table 2. Physical and engineering properties of tested soils.

Soil type:	Kaolinite	Bentonite
Source	Vanderbilt Co., Los Angeles, U.S.A.	Saskatchewan, Canada
Trade name	Peerless clay	Avonseal/Geoseal
Color	Light cream	Light tan
Specific gravity, G_s[a]	2.6	2.55
Specific surface, S (m^2/g)	10	400
Liquid limit (%)[a]	50	250
Plastic limit (%)[a]	35	50
CEC (mequiv./100 g)	10–20	80–85
Main cation in pore fluid[b]	Sodium	Sodium
Main adsorbed cation[c]	na	Sodium–calcium
pH value[d]	4.8 (10% solids)	9.0 (5% solids)
Conductivity[d] (S/m)	0.004 (10% solids)	0.112 (5% solids)

Notes: Values provided by suppliers unless specified. CEC, cation exchange capacity.
[a]University of Waterloo; standard ASTM procedure.
[b]University of Waterloo; ion chromatography on extracted fluid (bentonite: centrifuge; kaolinite: filtration).
[c]Data from Quigley (1984).
[d]University of Waterloo; solids in suspension.

Fig. 1. Change in coupling coefficients β, γ, and δ with the ratio between interparticle spacing and double-layer thickness $X = d/\vartheta$ (bentonite: A_s = 400 m^2/g, G_s = 2.55).

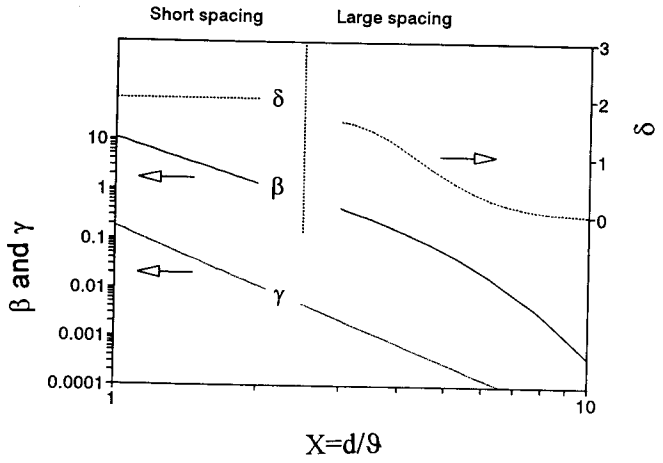

The coefficient β depends on soil properties (initial void ratio, soil compressibility, and specific surface) and pore-fluid characteristics (e.g., concentration and permittivity). The coefficient δ captures the sensitivity of the repulsion force to concentration.

Experimental study

Bentonite and kaolinite were selected for this study. Relevant engineering and physical properties are summarized in Table 2 (note the difference in specific surface). Kaolinite is in the upper limit of colloidal size, and manifests behavior not always predictable with double-layer and modified effective stress theories. On the other hand, the behavior of bentonite conforms to these theories.

Specimens were prepared using the slurry technique and were consolidated in a one-way drainage oedometer cell to a preselected vertical stress (see Fam and Santamarina 1995 for a detailed description of the cell). Sample height, pore-fluid pressure at the base, and imaginary dielectric permittivity at the base (at 1.30 GHz: coaxial probe) were recorded with time. After consolidation, a high concentration solution of KCl was allowed to diffuse through the specimen, keeping the vertical load constant.

Bentonite was consolidated to σ_v = 100 kPa before diffusion. Figure 2 presents a summary of the corresponding measurement set for bentonite, previously reported by Santamarina and Fam (1995). It is interesting to note the high pressure in the pore pressure front produced by the shrinkage of the skeleton ($\Delta u \approx 0.38\sigma$) and its arrival before the concentration front that caused it. Kaolinite was consolidated to σ_v = 610 kPa; diffusion caused a void ratio change from e_0 = 0.95 to e_f = 0.88. Again, the induced pore pressure front advanced ahead of the concentration front, but with a low peak value, $\Delta u \approx 0.003\sigma$.

Analysis

The following procedure was followed in the interpretation of experimental results, on the bases of the analytical formulation derived above.

Step 1: Diffusion coefficient and concentration field
The change in the relative imaginary permittivity κ'' is linearly related to the change in pore-fluid concentration. Thus, Fick's second law of diffusion can be rewritten in terms of κ'':

$$[18] \quad \frac{\partial c}{\partial t} = D\frac{\partial^2 c}{\partial z^2} \rightarrow \frac{\partial \kappa''}{\partial t} = D\frac{\partial^2 \kappa''}{\partial z^2}$$

Then, κ'' measurements are used to estimate by least-squares curve fitting the "apparent diffusion coefficient" D of the coupled diffusion process (eq. 18 is used in finite difference form; see Santamarina and Fam 1995). Measured and calculated imaginary permittivities at the base of the

sample are shown in Fig. 2*a*. The inverted diffusion coefficient is $D = 3 \times 10^{-10}$ m^2/s for bentonite (for kaolinite, $D = 5 \times 10^{-10}$ m^2/s). Given D, the variation of concentration with depth can be determined at any given time $c(z, t)$, using eq. 18.

Step 2: Coupling parameters

Once the spatial and temporal distribution of concentration $c(z, t)$ is known, eq. 12 can be numerically solved in finite difference form. Coefficients $c_v' = c_v(1 + \beta)$ and δ were determined by least squares fitting the pore pressure data measured at the base of the sample, u(base, t). The trend in continuous line in Fig. 2*b* was computed assuming constant coupling parameters during diffusion, obtaining $c_v' = 17 \times 10^{-10}$ m^2/s and $\delta \approx 0.25$ (the computed δ varies from $\delta = 1.08$ before diffusion to $\delta = 0.04$ after diffusion). However, concentration and void ratio are changing. Results presented in dotted lines in Fig. 2*b* were obtained by allowing for changes in δ and β, as predicted by $c(\kappa'')$ measurements. The reduction in double-layer thickness with the propagation of the concentration front, and the corresponding increase in hydraulic permeability may also be responsible for deviations between model and experimental data (see Mesri and Olsen 1971).

Step 3: Pore pressure field

The spatial distribution of pore pressure within the sample at any time $u(z, t)$ can be evaluated with eq. 12 knowing $c(z, t)$, c_v', and δ. Figure 3 shows the predicted spatial distribution of pore pressure and imaginary permittivity κ'' (linearly related to concentration) along the sample height at a specific time during diffusion. Figs. 2*a* and 2*b*, and Fig. 3 confirm that the pore pressure front advances ahead of the concentration front.

Step 4: Prediction of void ratio changes

The change in void ratio can be estimated by taking into consideration the change in concentration and in pore pressure. It follows from eq. 10,

$$[19] \quad \frac{\partial e}{\partial t} = \left(\frac{a_v}{1+\beta-\gamma}\right)\frac{\partial u}{\partial t} - \left(\frac{a_v \delta RT}{1+\beta-\gamma}\right)\frac{\partial c}{\partial t}$$

where a_v is the coefficient of compressibility; C_c was assumed constant before and during diffusion. Hence, the change in void ratio $e(z, t)$ can be calculated with the estimated distributions of concentration $c(z, t)$ and pore pressure $u(z, t)$. The predicted time-dependent settlement or average void ratio in the sample is computed from $e(z, t)$ and is plotted in Fig. 2*c*. The measured average void ratio is shown for comparison.

Discussion: Reassessment of assumptions

Barbour and Fredlund (1989) recognized the coupling between fluid characteristics, fabric changes, and fluid flow. However, they developed their model from a macroscopic perspective, linking volume changes to: (*i*) changes in effective stress through the conventional coefficient of compressibility a_{vc}, and (*ii*) changes in osmotic pressure

Fig. 2. Measured and calculated changes during KCl diffusion at $\sigma_v = 100$ kPa: (*a*) imaginary permittivity at the base of the sample, (*b*) pore-fluid pressure at the base of the sample, and (*c*) average void ratio.

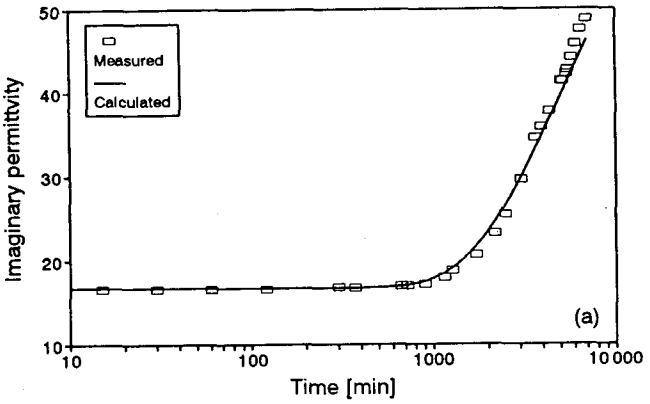

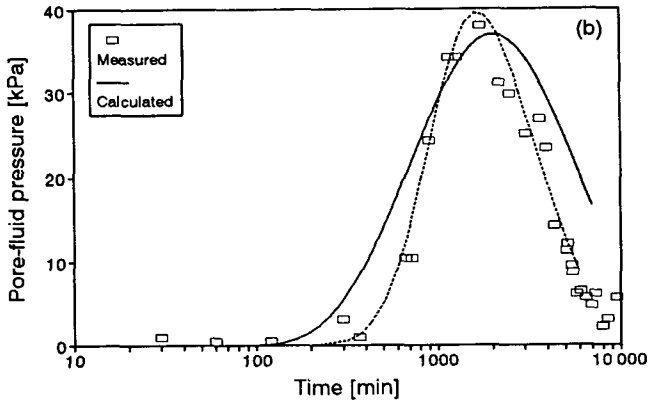

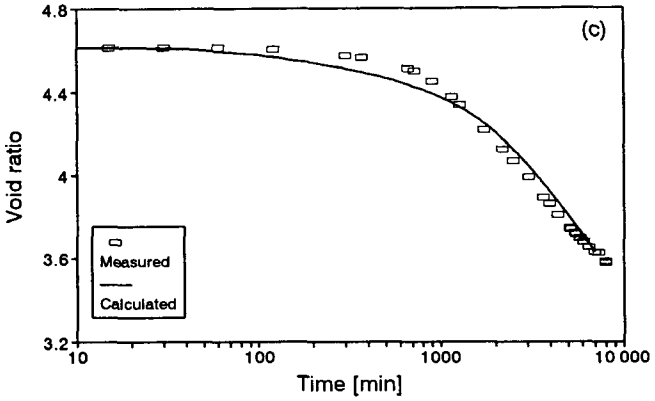

$\Pi = RTc$ through a "coefficient of osmotic compressibility" a_π:

$$[20] \quad \frac{\partial e}{\partial t} = a_{vc}\frac{\partial u}{\partial t} - a_\pi \frac{\partial \Pi}{\partial t} = a_{vc}\frac{\partial u}{\partial t} - a_\pi RT\frac{\partial c}{\partial t}$$

The comparison of eq. 19 and eq. 20 shows the following:

Fig. 3. Computed distribution of imaginary permittivity (concentration) and pore-fluid pressure along the sample height 7 h after the initiation of diffusion (back-calculated diffusion coefficient $D = 3 \times 10^{-10}$ m^2/s).

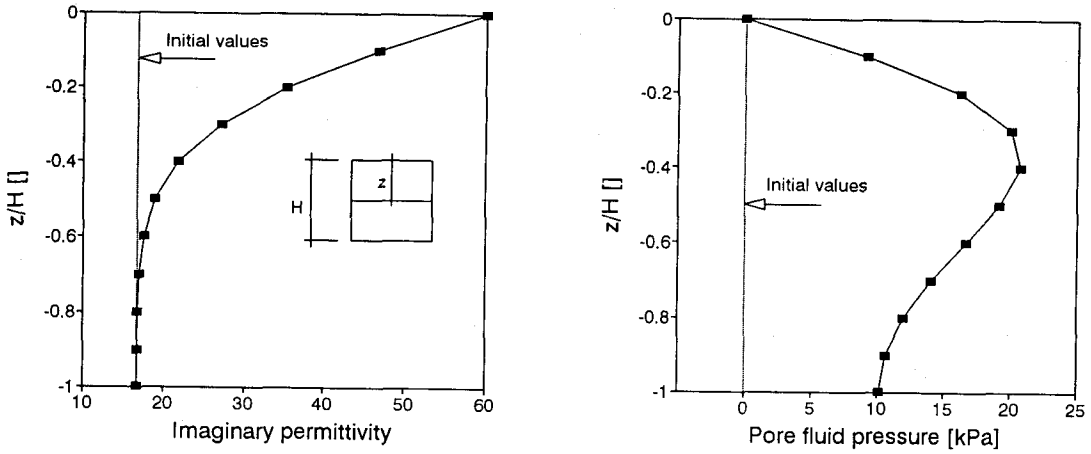

(1) The conventional coefficient of compressibility a_{vc} implicitly includes β and γ variables, which reflect long-range interparticle forces: $a_{vc} = a_v/(1 + \beta - \gamma)$. The same argument applies to the conventional coefficient of consolidation, where, the traditional experimental method gives the compounded value $c_{vc} = c_v(1 + \beta - \gamma)$. The difference between c_{vc} and c_v is significant in clays with high specific surface and low ionic concentration.

(2) The coefficient of osmotic compressibility a_π, for the assumed case of a fully dispersed clay depends on soil compressibility, specific surface, void ratio, and pore-fluid concentration: $a_\pi = a_{vc}\delta$. It is readily seen that the ratio a_π/a_{vc} is not a constant, but varies with the interparticle separation and the characteristics of the fluid. The dimensionless coefficient δ varies between 0.0001 and 2. This range includes the value measured by Barbour and Fredlund (1989), $\delta = 0.005$.

Barbour and Fredlund (1989) made the distinction between osmotic consolidation (the theme of this study) and osmotically induced consolidation, where negative pore pressure develops as pore fluid migrates to equilibrate a high concentration at the boundary. This second phenomenon was not observed in our study. It appears that the positive pore-fluid pressure front produced by osmotic consolidation overwhelms the negative pore-fluid pressure in soft soils.

The analysis conducted for bentonite was repeated with data obtained with the kaolinite specimen. Once again, the predicted pore pressure front preceded the concentration front, in agreement with measurements. The small measured changes in pore pressure ($\Delta u \approx 0.003\sigma$) indicate small coupling coefficients β and δ and fast pore pressure dissipation (high c_v).

Note that the analysis assumes that fluid–fabric-flow coupling is controlled by the rate of ionic diffusion into the soil mass (step 1 – eq. 18). Experimental results confirm this hypothesis.

In this study, the compression index $C_c = \Delta e/\Delta\log(p)$ was assumed constant before and during diffusion. However, C_c is likely to change during diffusion (the slope of e–$\log(p)$ curve is not necessarily equal to the slope of the e–$\log(R_{DL})$ curve).

The inverted coefficient of consolidation during diffusion is higher than c_v measured during consolidation before diffusion. Two opposite mechanisms control the actual value of c_v: the decline in double-layer thickness, which increases the effective permeability; and the decrease in porosity due to osmotic consolidation.

There are other coupling phenomena whereby the coupled response precedes the causing event. For example, the propagation of a mechanical wave in a thermoelastic medium may cause a thermal front ahead of the strain front (Achenbach 1973). Mathematically, this effect can be attributed to the nature of the diffusion equation, which predicts immediate spatial effects. However, results with modified diffusion formulations also show a preceding thermal front depending on relative material parameters.

This analysis is applicable to a variety of geotechnical engineering scenarios, including geoenvironmental cases such as clay liners designed to contain brine or organic materials, petroleum geomechanics and the effect of drilling muds on borehole instability, and civil infrastructure, such as the sensitivity assessment of embankment cores subjected to changes in reservoir characteristics.

Conclusions

Various modifications to Terzaghi's effective stress principle have been proposed to account for the compressibility of phases and electrical forces. Present models cannot satisfactorily describe both compressibility and shear strength. In part, restrictions reflect the grouping in one entity of parameters that correspond to different scales.

A simple mathematical framework was organized to evaluate the coupling of chemical and hydraulic fronts through changes in the soil skeleton. The selected effective stress model assumes that electrical and mechanical contact forces act in parallel. It was shown that the traditional coefficient of compressibility and the coefficient of consolidation include

the contribution of repulsion and attraction stresses, which are related to the physico-chemical properties of the clay. The proposed semicoupled analytical model predicted salient features of observed phenomena.

The model is based on interparticle forces and relates the analytical solution to micro-level parameters, allowing better insight into the relative role of participating variables. However, difficulties in upscaling to macro parameters is recognized.

The propagation of a concentration front through clays triggers the generation of a pore pressure front that precedes the concentration front. The increase in pore pressure may be important depending on the significance of the double-layer phenomena, the initial void ratio, and the compressibility of the soil skeleton.

These phenomena are present in a broad range of geotechnical engineering applications with different degrees of significance. The proposed analytical framework can be readily applied to assess diffusion–fabric-flow coupling in these cases.

Acknowledgments

This study is part of a research program on the behavior of particulate materials. Funding was provided by Natural Sciences and Engineering Research Council of Canada (NSERC). The authors are grateful to the reviewers for their insightful comments and suggestions.

References

Achenbach, J.D. 1973. Wave propagation in elastic solids. North-Holland Publishing Company, Amsterdam.

Allam, M.M., and Sridharan, A. 1984. The shearing resistance of saturated clays. Géotechnique, **34**: 119–122.

Barbour, S.L., and Fredlund, D.G. 1989. Mechanisms of osmotic flow and volume change in clay soils. Canadian Geotechnical Journal, **26**: 551–562.

Biot, M.A. 1941. General theory for three dimensional consolidation. Journal of Applied Physics, **12**: 155–164.

Bolt, G.H. 1956. Physico-chemical analysis of the compressibility of pure-clays. Géotechnique, **6**: 86–93.

Carroll, M.M., and Katsube, N. 1983. The role of Terzaghi effective stress in linearly elastic deformation. Journal of Energy Resources Technology, **105**: 509–511.

Chopra, M.B., and Dargush, G.F. 1995. Boundary element analysis of stresses in an axisymmetric soil mass undergoing consolidation. International Journal for Numerical and Analytical Methods in Geomechanics, **19**: 195–218.

Cryer, C.W. 1963. A comparison of the three-dimensional consolidation theories of Biot and Terzaghi. Quarterly Journal of Mechanics and Applied Mathematics, **XVI**: 401–411.

Fam, M., and Santamarina, J.C. 1995. Study of geoprocesses with complementary mechanical and electromagnetic wave measurements in an oedometer. ASTM Geotechnical Testing Journal, **18**: 307–314.

Hueckel, T. 1992. On effective stress concepts and deformation in clays subjected to environmental loads: Discussion. Canadian Geotechnical Journal, **29**: 1120–1125.

Ishibashi, I., Perry, C., III, and Agarwal, T.K. 1994. Experimental determinations of contact friction for spherical glass particles. Soils and Foundations, **34**: 79–84.

Israelachvili, J. 1991. Intermolecular and surface forces. Academic Press, London.

Lambe, W. 1960. A mechanistic picture of shear strength in clay. Soil Shear Strength Conference, Colorado, pp. 555–580.

Mesri, G., and Olsen, R.E. 1971. Consolidation characteristics of montmorillonite. Géotechnique, **21**(4): 341–352.

Mitchell, J.K. 1993. Fundamentals of soil behavior. 2nd ed. John Wiley & Sons, New York.

Nur, A., and Byerlee, J.D. 1971. An exact effective stress law for elastic deformation of rock with fluids. Journal of Geophysical Research, **76**(26): 6414–6419

Oka, F. 1988. The validity of the effective stress concept in soil mechanics. *In* Micromechanics of granular materials. *Edited by* M. Satake and J.T. Jenkins. Elsevier Science Publications, Amsterdam, pp. 207–214.

Quigley, R.M. 1984. Quantitative mineralogy and preliminary pore-water chemistry of candidate buffer and backfill materials for a nuclear fuel waste disposal site. Atomic Energy of Canada Limited, Whiteshell Nuclear Research Establishment, Pinawa, Manitoba.

Santamarina, J.C., and Fam, M. 1995. Changes in dielectric permittivity and shear wave velocity during concentration diffusion. Canadian Geotechnical Journal, **32**(4): 647–659.

Skempton, A.W. 1960. Effective stress in soils, concrete and rocks. Proceedings of a Conference on Pore Pressure and Suction in Soils. Butterworths, London, pp. 4–16.

Skinner, A.E. 1969. A note on the influence of interparticle friction on the shearing resistance of a random assembly of spherical particles. Géotechnique, **19**(1):150–157.

Spencer, J.W. 1981. Stress relaxations at low frequencies in fluid-saturated rocks: attenuation and modulus dispersion. Journal of Geophysical Research, **86**(B3): 1803–1812.

Sridharan, A., and Rao, V.G. 1973. Mechanisms controlling volume change of saturated clays and the role of effective stress concept. Géotechnique, **23**(3): 359–382.

Terzaghi, K. 1936. The shearing resistance of saturated soils and the angle between the planes of shear. Proceedings of the 1st International Conference on Soil Mechanics and Foundation Engineering, Vol. 1, pp. 54–56.

Yong, R.N., and Warkentin, B.P. 1966. Introduction to soil behavior. Macmillan Co., New York.

Appendix A: Solution for small interparticle spacing

Equation 2 is differentiated with respect to time to obtain (isothermal condition)

$$[A1] \quad \frac{\partial R_{DL}}{\partial t} = -8\pi^2 RT \frac{c\vartheta^2}{d^3}\frac{\partial d}{\partial t} - 2RT\frac{\partial c}{\partial t}$$

The change in d with time is proportional to the change in e (eq. 4),

$$[A2] \quad \frac{\partial d}{\partial t} = \frac{2}{A_s G_s \rho_w}\frac{\partial e}{\partial t} = -\frac{2a_v}{A_s G_s \rho_w}\frac{\partial \sigma'}{\partial t}$$

replacing back into A1,

$$[A3] \quad \frac{\partial R_{DL}}{\partial t} = +\frac{16\pi^2 a_v RT}{A_s G_s \rho_w}\frac{c\vartheta^2}{d^3}\frac{\partial \sigma'}{\partial t} - 2RT\frac{\partial c}{\partial t}$$

On the other hand, the time derivative of Att (eq. 6) is obtained by assuming that Hameker's constant is little sensitive to changes in concentration.

$$[A4] \quad \frac{\partial \mathrm{Att}}{\partial t} = \frac{-A}{2\pi d^4}\frac{\partial d}{\partial t} = \frac{a_v A}{\pi A_s G_s \rho_w d^4}\frac{\partial \sigma'}{\partial t}$$

Substituting A3 and A4 in eq. 10:

$$[A5]\quad \frac{\partial\sigma'}{\partial t} = -\frac{\partial u}{\partial t} - \frac{16\pi^2 a_v RT}{A_s G_s \rho_w}\frac{c\vartheta^2}{d^3}\frac{\partial\sigma'}{\partial t} + 2RT\frac{\partial c}{\partial t} + \frac{a_v A}{\pi A_s G_s \rho_w d^4}\frac{\partial\sigma'}{\partial t}$$

$$[A6]\quad \frac{\partial\sigma'}{\partial t}\left(1 + \frac{16\pi^2 a_v RT}{A_s G_s \rho_w}\frac{c\vartheta^2}{d^3} - \frac{a_v A}{\pi A_s G_s \rho_w d^4}\right) = -\frac{\partial u}{\partial t} + 2RT\frac{\partial c}{\partial t}$$

Assuming that the standard c_v coefficient applies to the coupled processes, then $\partial\sigma'/\partial t$ can be substituted by eq. 9.

$$[A7]\quad c_v\frac{\partial^2 u}{\partial z^2}\left(1 + \frac{16\pi^2 a_v RT}{A_s G_s \rho_w}\frac{c\vartheta^2}{d^3} - \frac{a_v A}{\pi A_s G_s \rho_w d^4}\right) = \frac{\partial u}{\partial t} - 2RT\frac{\partial c}{\partial t}$$

which can be written as

$$[A8]\quad \frac{\partial u}{\partial t} - \delta RT\frac{\partial c}{\partial t} = c_v(1 + \beta - \gamma)\frac{\partial^2 u}{\partial z^2}$$

where

$$\beta = \frac{16\pi^2\alpha}{X^3},\ \delta = 2,\ \alpha = \frac{ca_v RT}{A_s G_s \rho_w \vartheta},\ \gamma = \frac{a_v A}{\pi A_s G_s \rho_w (X\vartheta)^4},$$

and

$$X = \frac{d}{\vartheta}$$

A similar equation can be written for large spacing (eq. 3),

$$[A9]\quad \frac{\partial u}{\partial t} - \delta' RT\frac{\partial c}{\partial t} = c_v(1 + \beta' - \gamma)\frac{\partial^2 u}{\partial z^2}$$

where $\beta' = 128\alpha e^{-X}$ and $\delta' = 64\left(\frac{X}{2} - 1\right)e^{-X}$